Progress In Electromagnetics Research, PIER 79, 107–118, 2008

AN EXACT SOLUTION OF COHERENT WAVE PROPAGATION IN RAIN MEDIUM WITH REALISTIC RAINDROP SHAPES

M. Bahrami, J. Rashed-Mohassel, and M. Mohammad-Taheri

Center of Excellence on Applied Electromagnetic Systems
ECE Department
University of Tehran
Tehran, Iran

Abstract—Computation of coherent electromagnetic wave propagation through rain medium with a realistic raindrop shape is the subject of this work. T-Matrix approach towards the computation of forward scattering amplitude of raindrops is considered numerically exact. The results of Total Cross Section and forward scattering amplitude due to raindrops with MPP model shape are calculated by T-Matrix method. Both horizontal and vertical polarization of incident wave are considered where specific attenuation, phase shift and cross polarization discrimination (XPD) for terrestrial coherent electromagnetic wave propagation in the frequency range of 3–300 GHz are presented. Furthermore the effect of temperature on specific attenuation vs. frequency is investigated.

1. INTRODUCTION

The performance of communication links, in frequencies above 5 GHz, especially in the microwave or millimeter wave range, used in terrestrial repeater or earth satellite communication systems are affected by hydrometeors attenuation [1–4]. In this paper we consider the effect of falling raindrops on coherent wave propagation due to its dominant effects, with respect to the other hydrometeors such as snow, fog and hail, on millimeter wave propagation.

Falling raindrops have, in general, nonspherical shapes due to aerodynamic and gravitational forces. In most of efforts, the oblate spheroid shape is considered for raindrop shape models [5]. There are two linear relation nominations, line A, with equation "$a/b = 1-0.1a_o$"

and line B, with $(a/b = 1 - (0.41/4.5)a_o)$ which are used for axial ratio calculations. In these equations, a_o is equal to the raindrop mean radius in millimeters and a nonlinear equation for axial ration is assumed as [6]:

$$a/b = \begin{cases} 1 & r_{eqv} \leq 0.05\,\text{cm} \\ 1.0048 + 0.0114 r_{eqv} - 10.512 r_{eqv}^2 + 29.456 r_{eqv}^3 - 26.832 r_{eqv}^4 & 0.05\,\text{cm} < r_{eqv} \leq 0.45\,\text{cm} \end{cases} \quad (1)$$

On the other hand, a typical and accepted model for realistic describing of raindrop shapes was developed by Pruppacher and Pitter (PP model) [7], who solved a pressure balance equation on the surface of raindrops by numerical techniques and determined their shapes for various sizes. Oguchi [7] used the cosine series function to replace PP nonlinear equations with simple functions and Li et al. used a different functional expression further simplify the PP model for the calculation of rain attenuation which is known as Modified PP (MPP) model [9]. Figure 1 shows the normalized shape of realistic and oblate spheroid raindrops with axial ratio given by Equation (1).

De Wolf and Zwiesler used the Rayleigh-Mie approximation to predict the rain attenuation and phase changes [11]. Various numerical techniques such as Perturbation method was proposed by Oguchi [10] and utilized by Li et al. [12]. Other methods such as Least square fitting method, Unimoment [13], method of moments [14], spheroidal function expansion [15], Fredholm integral equation method [16], T-Matrix method [17] and some other were introduced [18] and were used for computation of scattering properties by raindrops. To the best of our knowledge, the shape of rain drops is assumed to be oblate spheroid in many of the above efforts and any exact solution for scattering properties of realistic MPP raindrop shapes is not presented. Hence, the T-Matrix method is investigated for the exact calculation of forward scattering amplitude of realistic raindrops.

2. THEORY

The incident and scattered fields inside and outside of circumscribing sphere are expanded in vector spherical wave functions $\vec{M}_{mn}$ and $\vec{N}_{mn}$

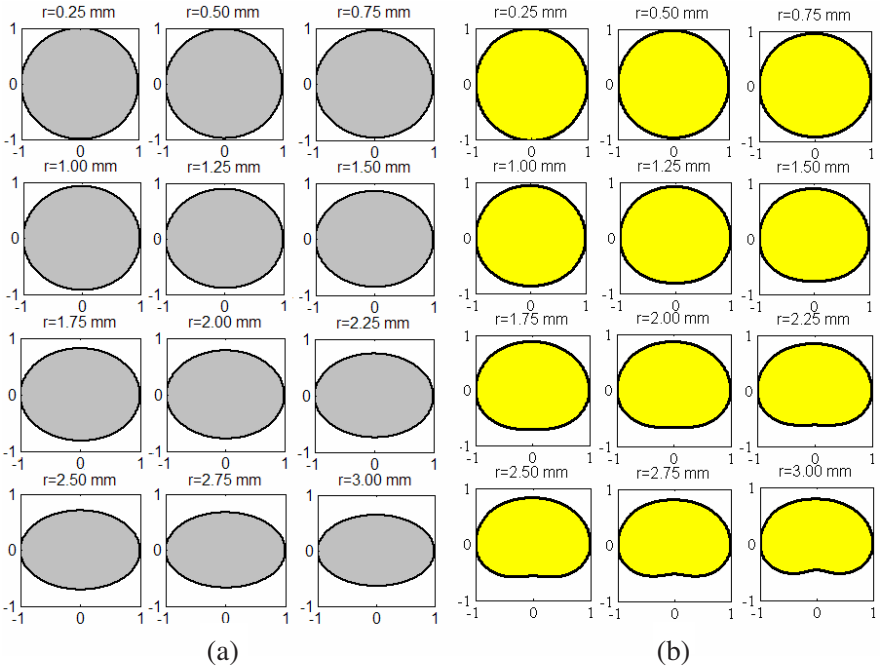

Figure 1. (a) Oblate spheroid raindrops shapes with axial ratio given by Equation (1), (b) Realistic raindrops shapes (MPP model) [9].

in the framework of T-Matrix as follows:

$$\vec{E}^{inc}(\vec{r}) = \sum_{n=1}^{\infty} \sum_{m=-n}^{n} \left[a_{mn} Rg\vec{M}_{mn}(kr,\theta,\varphi) + b_{mn} Rg\vec{N}(kr,\theta,\varphi) \right] \quad r < r_c \tag{2}$$

$$\vec{E}^{sca}(\vec{r}) = \sum_{n=1}^{\infty} \sum_{m=-n}^{n} \left[p_{mn} \vec{M}_{mn}(kr,\theta,\varphi) + q_{mn} \vec{N}(kr,\theta,\varphi) \right] \quad r > r_c \tag{3}$$

Because of the linearity of Maxwell's equations and boundary conditions, the relation between the scattered field coefficients, p_{mn} and q_{mn} and incident fields coefficients, a_{mn} and b_{mn} are given by:

$$p_{mn} = \sum_{n'=1}^{\infty} \sum_{m'=-n'}^{n'} \left[T^{11}_{mnm'n'} a_{m'n'} + T^{12}_{mnm'n'} b_{m'n'} \right] \tag{4}$$

$$q_{mn} = \sum_{n'=1}^{\infty} \sum_{m'=-n'}^{n'} \left[T^{21}_{mnm'n'} a_{m'n'} + T^{22}_{mnm'n'} b_{m'n'} \right] \tag{5}$$

which can be rewritten in the matrix form:

$$\begin{bmatrix} p \\ q \end{bmatrix} = T \begin{bmatrix} a \\ b \end{bmatrix} = \begin{bmatrix} T^{11} & T^{12} \\ T^{21} & T^{22} \end{bmatrix} \begin{bmatrix} a \\ b \end{bmatrix}. \tag{6}$$

The internal field can be expanded in vector spherical function as follows:

$$\vec{E}^{int}(\vec{r}) = \sum_{n=1}^{\infty} \sum_{m=-n}^{n} \left[c_{mn} Rg\vec{M}_{mn}(m_r kr, \theta, \varphi) + d_{mn} Rg\vec{N}(m_r kr, \theta, \varphi) \right] \tag{7}$$

where, m_r is the refractive index of the particle relative to that of the surrounding medium. The relation between the expansion coefficients of the incident and scattered fields with the internal field is linear and is given by:

$$\begin{bmatrix} a \\ b \end{bmatrix} = \begin{bmatrix} Q^{11} & Q^{12} \\ Q^{21} & Q^{22} \end{bmatrix} \begin{bmatrix} c \\ d \end{bmatrix} \tag{8}$$

$$\begin{bmatrix} p \\ q \end{bmatrix} = - \begin{bmatrix} RgQ^{11} & RgQ^{12} \\ RgQ^{21} & RgQ^{22} \end{bmatrix} \begin{bmatrix} c \\ d \end{bmatrix} \tag{9}$$

Finally, elements of the T-Matrix can be calculated as:

$$T = -(RgQ)\, Q^{-1} \tag{10}$$

With respect to the elements of T-Matrix and the far field approximation, the elements of scattering amplitude matrix can be readily computed.

There are some relations between T-Matrix elements for axisymmetric particles such as realistic or oblate spheroid raindrops which can simplify the calculation procedure as:

$$\begin{aligned} T^{ij}_{mnm'n'} &= \delta_{mm'} T^{ij}_{mnmn'} \quad i,j = 1,2 \\ T^{ij}_{-mn-mn'} &= (-1)^{i+j} T^{ij}_{mnmn'} \quad i,j = 1,2 \\ T^{12}_{0n0n'} &= 0 \\ T^{21}_{0n0n'} &= 0 \end{aligned} \tag{11}$$

Since in rain medium there are raindrops with various radii, it is necessary to take into account the drop size distribution. The propagation constant for coherent wave K in rain medium is given

by [19]

$$K_\alpha = k + \frac{2\pi}{k} \langle f_{\alpha\alpha} (\hat{n}_{inc}, \hat{n}_{inc}) \rangle , \tag{12a}$$

$$\langle f_{\alpha\alpha} (\hat{n}_{inc}, \hat{n}_{inc}) \rangle = \int_0^\infty f_{\alpha\alpha} (\hat{n}_{inc}, \hat{n}_{inc}) \mathrm{N} (r, RR)\, dr \tag{12b}$$

$\mathrm{N}(r, RR)$ shows the number of raindrops with an average radii from r to $r + dr$ per unit volume while the rain rate equals RR [5, 9]. $f_{\alpha\alpha} (\hat{n}_{inc}, \hat{n}_{inc})$ is forward scattering amplitude when polarization of incident and scattered waves is α. According to Equation (12), specific attenuation ($A^{v,h}$) and phase shift ($\varphi^{v,h}$) of vertical and horizontal coherent wave through a path of length L are given by

$$A^{v,h} = 1000 (\log_{10} e) \langle \sigma_{v,h} \rangle \text{ dB}, \tag{13a}$$

$$\varphi^{v,h} = \frac{180}{\pi} \mathrm{Re} (K_{v,h} L) \text{ deg} . \tag{13b}$$

In Equation (13a), $\langle \sigma_{v,h} \rangle$ is ensemble average of total cross section. The axis of symmetry of falling raindrops is not aligned with the vertical direction and cant from the vertical direction due to various aerodynamic forces acting on falling raindrops. Since it is suitable to calculate forward scattering amplitude in raindrop symmetry coordinates, it is necessary to convert propagation coordinate to raindrop symmetry coordinates and vise versa. Figure 2 shows these two coordinates and canting angle of falling raindrops.

The received wave due to incident wave in propagation coordinate

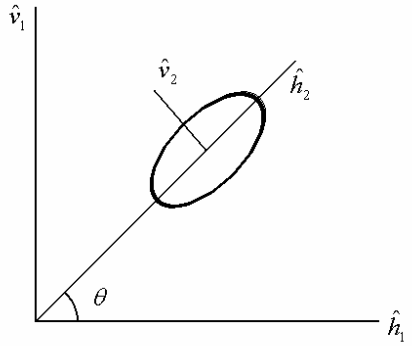

Figure 2. Propagation and raindrop symmetry coordinates.

is then given by

$$\begin{bmatrix} E_{v1}^r \\ E_{h1}^r \end{bmatrix} = \begin{bmatrix} \cos\theta & \sin\theta \\ -\sin\theta & \cos\theta \end{bmatrix} \begin{bmatrix} \exp(jK_{v2}L) & 0 \\ 0 & \exp(jK_{h2}L) \end{bmatrix} \begin{bmatrix} \cos\theta & -\sin\theta \\ \sin\theta & \cos\theta \end{bmatrix} \begin{bmatrix} E_{v1}^{inc} \\ E_{h1}^{inc} \end{bmatrix} \quad (14)$$

where θ is the canting angle. Cross polarization discrimination (XPD) can be defined as $XPD_h = 20\log_{10}|E_{v1}^r/E_{h1}^r|$ when incident wave has horizontal polarization and as $XPD_v = 20\log_{10}|E_{h1}^r/E_{v1}^r|$, when incident wave has vertical polarization. Using Equation (14), we have

$$XPD_h = 20\log\left|\frac{\frac{\sin 2\theta}{2}\left(\exp(jK_{h2}L) - \exp(jK_{v2}L)\right)}{\sin^2\theta\exp(jK_{v2}L) + \cos^2\theta\exp(jK_{h2}L)}\right|, \quad (15a)$$

$$XPD_v = 20\log\left|\frac{\frac{\sin 2\theta}{2}\left(\exp(jK_{h2}L) - \exp(jK_{v2}L)\right)}{\sin^2\theta\exp(jK_{h2}L) + \cos^2\theta\exp(jK_{v2}L)}\right| \quad (15b)$$

3. RESULTS

Electromagnetic scattering by realistic and oblate spheroidal raindrop shapes are simulated with the T-Matrix approach. The convergence of the program is tested with fixed and random orientated total cross sections and forward scattering amplitude criteria.

Figure 3 shows the convergence procedure of horizontal and vertical Total Cross Sections (TCS) of realistic raindrop shapes with a 2 mm equal average radius at 30 GHz and 20°C. The angle of incidence of the plane wave is 90 degrees.

As can be seen, The TCS for realistic raindrop has an accurate value up to 6 significant digits.

The Total cross section and forward scattering amplitude for realistic and oblate spheroidal raindrop models were also simulated in the frequency range of 3–300 GHz and the Specific attenuation, XPD and phase shift of different models were calculated.

Figure 4 shows the difference between horizontal specific attenuation and vertical specific attenuation vs. frequency. The rain rate is 15 mm/h for Marshall-palmer drop size distribution [5] and the dielectric constant of water is calculated by Double-Debay approximation [20, 21] at 20°C.

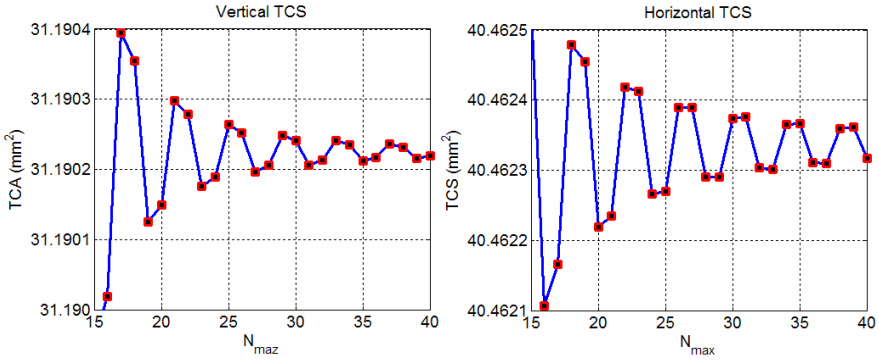

Figure 3. Convergence of horizontal and vertical TCS at 30 GHz and 20°C.

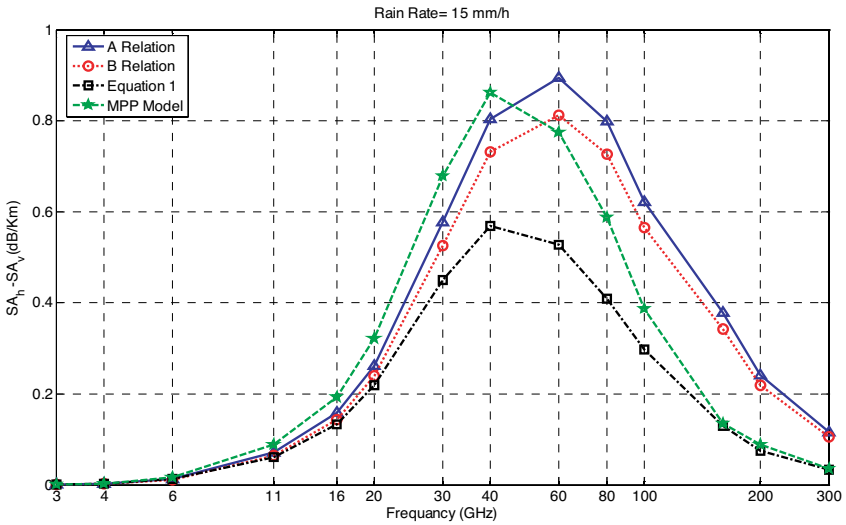

Figure 4. The difference between horizontal specific attenuation and vertical specific attenuation vs. frequency.

It can be observed that the difference between horizontal and vertical specific attenuations at the frequencies of 30–60 GHz is maximum. In fact, the mean dimensions of raindrops are comparable to wavelength which is named resonance regime. At very high or very low frequencies, we are at optical and Rayleigh regime respectively, and the difference between vertical and horizontal polarization is a minimum.

Figure 5 shows the difference of horizontal phase shift and vertical phase shift vs. frequency at the rain rate of 15 mm/h and the dielectric constant of water at 20°C.

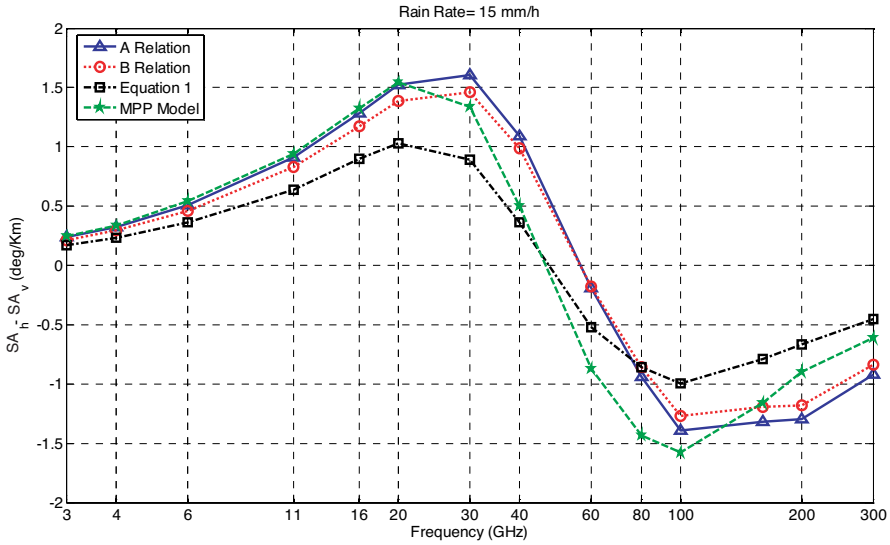

Figure 5. The difference between horizontal phase shift and vertical phase shift.

Figures 6(a) and 6(b) show the horizontal and vertical XPD vs. frequency for 5 km path length and 25 millimeter per hour rain rate respectively. Canting angle is assumed to be 5 degree.

Similar to the mentioned reasons which were described for the difference between horizontal and vertical specific attenuations, the horizontal and vertical XPD also follow the same method. It means that, not only the vertical XPD and the horizontal XPD by themselves, but also, the difference of Horizontal and vertical XPD in Figures 6(a) and 6(b) become a maximum at frequencies of 30–60 GHz and fall to a minimum at high and low frequencies.

The dielectric constant of water at different temperatures and frequencies are available in Table 1. It is obvious that the real and imaginary parts of the dielectric constant at frequencies about 1 GHz are decreased as the temperature increases. Also a complete inverse treatment is performed in 30 GHz and the real and imaginary parts are increased as temperature increases.

It should be noted that, close to 8 GHz, the real part of dielectric constant of water increases with an increase in temperature while the imaginary part decreases as temperature increases.

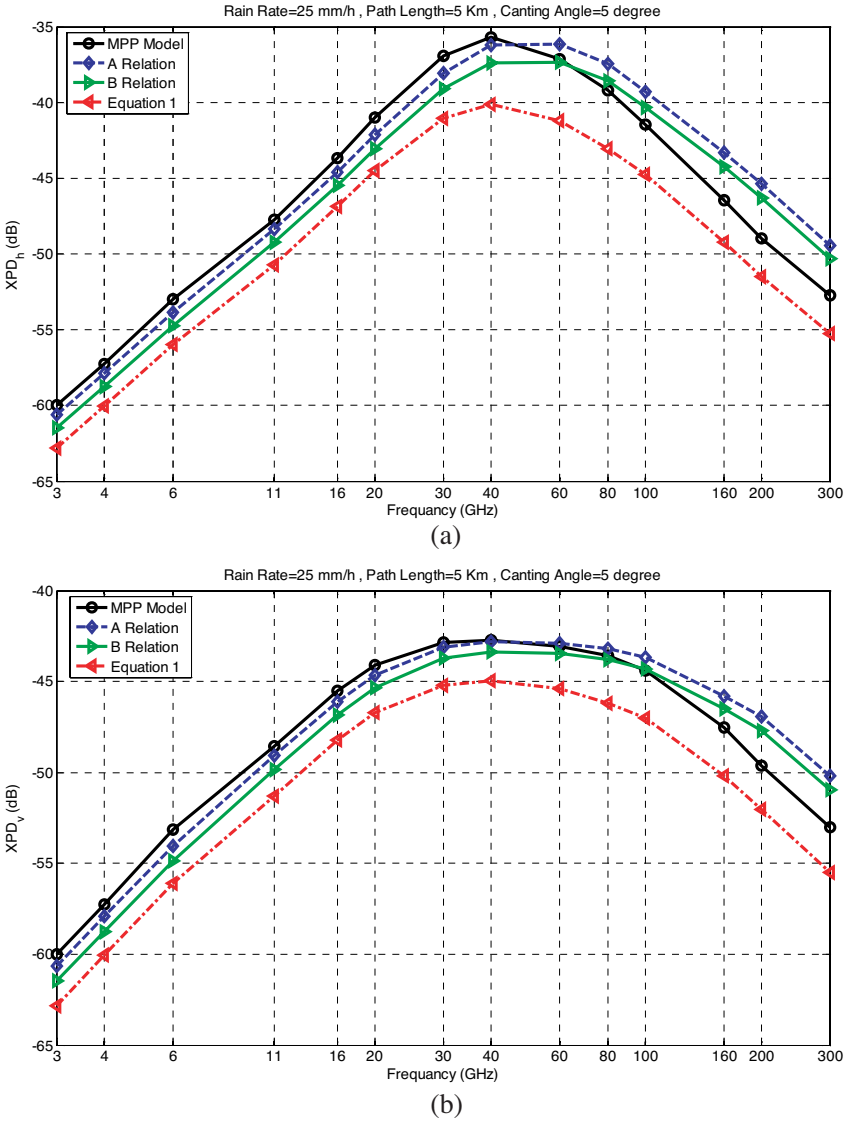

Figure 6. (a) Horizontal XPD and (b) Vertical XPD vs. frequency.

Figure 7 shows the variations of normalized vertical specific attenuation of realistic raindrops with respect to specific attenuation values at 25°C for different temperatures at frequency range of 1–40 GHz.

Table 1. Dielectric constant of water vs. temperature.

Temp (°C)	$F = 1$ GHz	$F = 8$ GHz	$F = 30$ GHz
0	86.834+j9.194	50.834+j40.870	12.3849+j22.432
10	83.371+j6.201	61.248+j35.5086	17.264+j28.0017
25	78.156+j3.793	67.570+j25.9397	26.5445+j33.280

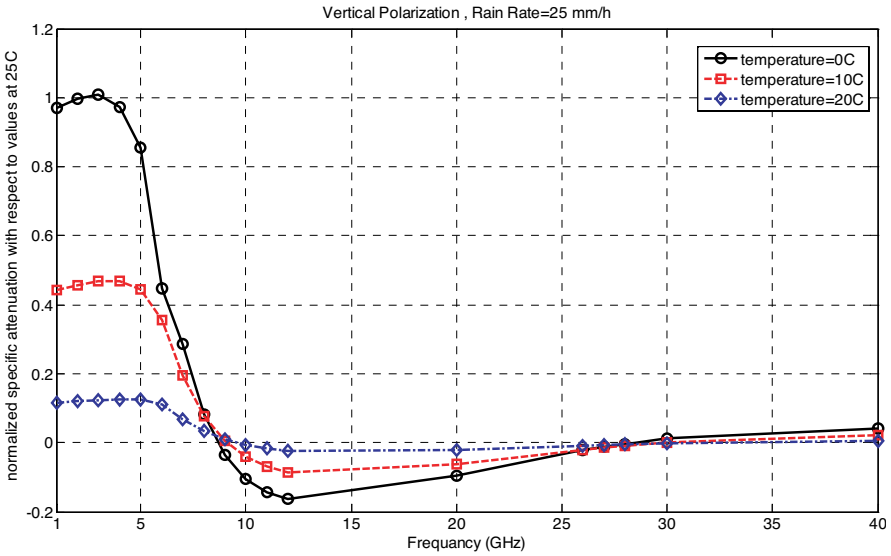

Figure 7. Normalized vertical specific attenuation of realistic raindrops with respect to specific attenuation values at 25°C.

It is observed that the value of specific attenuation is increased as the temperature decreases in around 1 GHz and 30 GHz, but in the middle frequencies and around 8 GHz, the specific attenuation increases as the temperature is increased. Variation of normalized horizontal specific attenuation of realistic raindrops with respect to specific attenuation values at 25°C is similar to those of vertical polarization.

4. CONCLUSION

An exact solution for millimeter wave scattering from nonspherical raindrops with T-Matrix method is presented. The forward scattering amplitude, total cross section for realistic and oblate spheroid raindrops were computed and the specific attenuation, phase shift, and XPD for vertical and horizontal polarizations are calculated. The results are appropriated in several plots and the temperature dependence of specific attenuation is also presented.

REFERENCES

1. Mandeep, J. S., "Rain attenuation predictions at Ku-band in South East Asia countries," *Progress In Electromagnetics Research*, PIER 76, 65–74, 2007.
2. Panagopoulos, A. D. and G. E. Chatzarakis, "Outage performance of single/dual polarized fixed wireless access links in heavy climatic regions," *J. of Electromagnetic Waves and Application*, Vo. 21, No. 3, 283–297, 2007.
3. Mandeep, J. S., "Equatorial rainfall measurements on Ku-band datellite communication downlink," *Progress In Electromagnetics Research*, PIER 76, 195–200, 2007.
4. Chen, K. S. and C. Y. Chu, "A propagation study of the 28 GHz LMDS system performance with M-QAM modulations under rain fading," *Progress In Electromagnetics Research*, PIER 68, 35–51, 2007.
5. Georgiadou, E. M., A. D. Panagopoulos, and J. D. Kaanellopoulos, "Millimeter wave pulse propagation through distorted raindrops for LOS fixed wireless access channels," *J. of Electromagnetic Waves and Application*, Vo. 20, No. 9, 1235–1248, 2006.
6. Battaglia, A., F. Prodi, and O. Sturniolo, "Radar and scattering parameters through falling hydrometeors with axisymmetric shapes," *Applied Optics*, Vol. 40, No. 18/20, 3092–3100, 2001.
7. Pruppacher, H. R. and R. L. Pitter, "A semi-empirical determination of the shape of cloud and rain drops," *Journal of the Atmospheric Science*, Vol. 28, 86–94, Jan. 1971.
8. Oguchi, T., "Scattering properties of Pruppacher-and-Pitter form rain-drops and cross polarization due to rain: Calculation at 11, 13, 19.3, and 34.8 GHz," *Radio Science*, Vol. 12, 41–51, 1977.
9. Li, L.-W., P.-S. Kooi, M.-S. Leong, T.-S. Yeo, and M.-Z. Gao, "Microwave attenuation by realistically distorted raindrops: Part I - Theory," *IEEE Trans. on AP*, Vol. 43, No. 8, 811–822, Aug. 1995.

10. De Wolf, D. A. and A. J. Zwiesler, "Rayleigh-Mie approximation for line-of-sigth propagation through rain at 5–90 GHz," *IEEE Trans. on AP*, Vol. 44, 273–279, Mar. 1996.
11. Oguchi, T., "Attenuation and phase rotation of radio waves due to rain: Calculations at 19.3 and 34.8 GHz," *Radio Science*, Vol. 8, No. 1, 31–38, 1973.
12. Li, L.-W., T.-S. Yeo, P.-S. Kooi, and M.-S. Leong, "An efficient calculation approach to evaluation of microwave specific attenuation," *IEEE Trans. on AP*, Vol. 48, No. 8, 1220–1229, Aug. 2000.
13. Ajose, S. O. and M. N. O. Sadiku, "Computation of attenuation, phase rotation, and cross-polarization of radio waves due to rainfall in tropical regions," *IEEE Trans. on AP*, Vol. 43, No. 1, 1–5, Jan. 1995.
14. Lin, D.-P. and H.-Y. Chen, "Volume integral equation solution of extinction cross section by raindrops in the range 0.6–100 GHz," *IEEE Trans. on AP*, Vol. 49, No. 3, 494–499, Mar. 2001.
15. Li, L.-W., T. S. Yeo, P. S. Kooi, and M. S. Leong, "Microwave specific attenuation by oblate spheroidal raindrops: an exact analysis of TCS's in terms of spheroidal wave functions," *Progress In Electromagnetics Research*, PIER 18, 127–150, 1998.
16. Holt, A. R., N. K. Uzunoglu, and B. G. Evans, "An integral solution to the scattering of electromagnetic radiation by dielectric spheroids and ellipsoids," *IEEE Trans. on AP*, Vol. 26, No. 5, 706–712, Sep. 1978.
17. Seow, Y. L., L.-W. Li, M.-S. Leong, P.-S. Kooi, and T.-S. Yeo, "An efficient TCS formula for rainfall microwave attenuation: T-Matrix approach and 3-D fitting for oblate spheroidal raindrops," *IEEE Trans. on AP*, Vol. 46, No. 8, 1176–1181, Aug. 1998.
18. Oguchi, T., "Electromagnetic wave propagation and scattering in rain and other hydrometeors," *Proc. IEEE*, Vol. 71, No. 9, 1029–1079, Sep. 1983.
19. Mishchenko, M. I., L. D. Travis, and A. A. Lacis, *Scattering Absorption, and Emission of Light by Small Particles*, Goddard Institute for Space Studies, New York, 2004.
20. ITU-R P.840-3, "Attenuation due to clouds and fogs," Oct. 1999.
21. Gong, S. H. and J. Y. Huang, "Accurate analytical model of equivalent dielectric constant for rain medium," *J. of Electromagnetic Waves and Application*, Vol. 20, No. 13, 1775–1783, 2006.